

ORIGINAL ARTICLE

Fucoidan-functionalized activated platelet-hitchhiking micelles simultaneously track tumor cells and remodel the immunosuppressive microenvironment for efficient metastatic cancer treatment



Rong Guo, Miao Deng, Xuan He, Mengmeng Li, Jiaxin Li,
Penghui He, Houqin Liu, Man Li, Zhirong Zhang, Qin He*

Key Laboratory of Drug-Targeting and Drug Delivery System of the Education Ministry and Sichuan Province,
Sichuan Engineering Laboratory for Plant-Sourced Drug and Sichuan Research Center for Drug Precision
Industrial Technology, West China School of Pharmacy, Sichuan University, Chengdu 610041, China

Received 27 January 2021; received in revised form 21 March 2021; accepted 19 April 2021

KEY WORDS

Fucoidan;
Activated platelets;
P-selectin;
Platelets-hitchhiking;
Track tumor cells;
TGF- β ;
Reverse
immunosuppressive
microenvironment;
Tumor metastasis

Abstract Tumor metastasis is responsible for most mortality in cancer patients, and remains a challenge in clinical cancer treatment. Platelets can be recruited and activated by tumor cells, then adhere to circulating tumor cells (CTCs) and assist tumor cells extravasate in distant organs. Therefore, nanoparticles specially hitchhiking on activated platelets are considered to have excellent targeting ability for primary tumor, CTCs and metastasis in distant organs. However, the activated tumor-homing platelets will release transforming growth factor- β (TGF- β), which promotes tumor metastasis and forms immunosuppressive microenvironment. Therefore, a multitalent strategy is needed to balance the accurate tumor tracking and alleviate the immunosuppressive signals. In this study, a fucoidan-functionalized micelle (FD/DOX) was constructed, which could efficiently adhere to activated platelets through P-selectin. Compared with the micelle without P-selectin targeting effect, FD/DOX had increased distribution in both tumor tissue and metastasis niche, and exhibited excellent anti-tumor and anti-metastasis efficacy on 4T1 spontaneous metastasis model. In addition, due to the contribution of fucoidan, FD/DOX

*Corresponding author. Tel./fax: +028 85502532.

E-mail addresses: qinhe@scu.edu.cn, qinhe317@126.com (Qin He).

Peer review under responsibility of Chinese Pharmaceutical Association and Institute of Materia Medica, Chinese Academy of Medical Sciences.

treatment was confirmed to inhibit the expression of TGF- β , thereby stimulating anti-tumor immune response and reversing the immunosuppressive microenvironment. The fucoidan-functionalized activated platelets-hitchhiking micelle was promising for the metastatic cancer treatment.

© 2022 Chinese Pharmaceutical Association and Institute of Materia Medica, Chinese Academy of Medical Sciences. Production and hosting by Elsevier B.V. This is an open access article under the CC BY-NC-ND license (<http://creativecommons.org/licenses/by-nc-nd/4.0/>).

1. Introduction

Metastasis is the major cause of cancer-associated mortality^{1–3}. Current clinical therapeutic options for cancer including surgery, irradiation and chemotherapy can remove local tumor; however, they can hardly act on metastasis^{4,5}. Therefore, effective anti-metastasis strategies are in urgent need and are crucial for clinical cancer treatment. The formation of metastasis in distant organs including lung and liver is a complicated multiphase process: first, tumor cells detached from the primary tumor enter the circulatory system to form circulating tumor cells (CTCs); then, survived CTCs translocate through the bloodstream to distant organs and extravasate there; finally, tumor cells colonize at new organs and proliferate to form a secondary tumor^{6–8}. The above metastatic cascade provides targets for anti-metastasis therapy.

Numerous studies revealed that platelets play a crucial role in the formation of metastasis through complex connections with tumor cells^{9,10}. In detail, platelets can be activated and recruited by tumor cells. Then, the activated platelets will secrete several factors, such as transforming growth factor- β (TGF- β), to increase tumor cell survival and promote metastasis¹¹. Furthermore, the activated platelets can adhere to CTCs as “protective coats” to assist the CTCs survive in blood circulation¹². Platelets also assist tumor cells extravasate and seed at distant organs¹³. These contributions of platelets provide new possibilities for cancer therapy.

In recent years, multiple platelet-mediated drug delivery platforms have been reported for cancer treatment¹⁴. Platelet engineering is a common strategy. For example, the monoclonal antibody against PDL1 was modified on the surface of platelets for cancer therapy^{15–17}. Nevertheless, *ex vivo* engineering is a complicated process, and it is hard to maintain the biological functions of engineered platelets for a long time. Besides, the injection of platelets probably leads to deterioration of cancer, since elevated platelet counts can cause tumor-related thrombosis and promote tumor development¹⁸. Coating nanoparticles with platelet membrane is another widely reported strategy^{19–21}. Unfortunately, since the *ex vivo* isolated platelet membrane is not exactly the same as internal platelets, the interaction between platelet-mimicking nanoparticles and tumor cells may be weak.

Therefore, *in vivo* intact activated platelet was considered to be a more attractive platform for drug delivery. *In vivo* activated platelets have upregulated expression of receptors, including GPIb-V-IX, Integrin α IIb β 3 and P-selectin²², which ensure the adhesiveness of platelets to perform subsequent functions in tumor metastasis. Thus, nanoparticles can hitchhike on activated platelets by targeting these receptors^{23,24}. As an example, PSN peptide (DAEWVDVS)-modified micelle has been developed for activated platelets targeting²⁵. The activated platelets-hitchhiking nanoparticles will track tumor cells through the “platelet bridge”. However, a serious problem that tumor-homing platelets can secrete TGF- β to promote tumor growth and metastasis remains

unsolved. Thus, the inhibition of TGF- β is important for the activated platelets-hitchhiking strategy. In fact, TGF- β is secreted by many types of cells, it will induce changes in the phenotype of tumor cells, and it is required for tumor cells colonization in premetastatic organs^{26,27}. TGF- β secreted by tumor cells also suppresses the anti-tumor immune response^{28,29}. Therefore, the inhibition of TGF- β will contribute to the anti-tumor and anti-metastasis effect by remodeling the microenvironment.

Fucoidan is a highly sulfated polysaccharide that exhibits nanomolar affinity for P-selectin^{30,31}. And the fucoidan-functionalized nanoparticles have been utilized to treat thrombosis and cardiovascular diseases with high expression of P-selectin^{31–33}. Therefore, the fucoidan-functionalized micelle is hypothesized to track tumor cells accurately by hitchhiking on activated platelet. More importantly, fucoidan is reported as a TGF- β inhibitor in liver fibrosis model³⁴, which may inhibit the TGF- β in primary tumor and premetastatic organs. Besides, fucoidan possesses an immunostimulatory function to enhance adaptive immune responses^{35–37}, holding the potential to remodel the immunosuppressive tumor microenvironment. In this study, a fucoidan-functionalized DOX-loaded micelle (FD/DOX) was developed to specifically hitchhike on activated platelets, and inhibit TGF- β at the same time. The binding affinity of FD/DOX with activated platelets was verified *in vitro*. The cellular uptake and cytotoxicity were conducted on 4T1 cells. The biodistribution, anti-tumor and anti-metastasis effect of FD/DOX were investigated on 4T1 spontaneous metastasis model. The tumor microenvironment reestablishment was also explored. Combined with immunogenic cell death (ICD) caused by chemotherapy drug DOX³⁸, FD/DOX is expected to stimulate potent anti-tumor immune responses, contributing to the metastatic cancer treatment.

2. Materials and methods

2.1. Materials

Fucoidan and thrombin were purchased from Yuanye Bio-Technology Co., Ltd. (Shanghai, China). Deoxycholic acid and dextran 10,000 were purchased from Solarbio Science & Technology Co., Ltd. (Shanghai, China). Doxorubicin hydrochloride (DOX·HCl) was purchased from Meilun Biological Technology Co., Ltd. (Dalian, China). *N*-Hydroxy-succinimide (NHS), 4-(dimethylamino) pyridine (DMAP), 1-[3-(dimethylamino) propyl]-3-ethylcarbodiimide hydrochloride (EDCI) and organic solvent dimethyl sulfoxide (DMSO) were purchased from J&K Scientific Co., Ltd. (Beijing, China). Formamide and *N,N*-dimethylformamide (DMF) were purchased from Adamas Reagent Co., Ltd. (Shanghai, China). Other chemicals were analytical level. Lyso-Tracker red, 3-(4,5-dimethyl-2-tiazolyl)-2,5-diphenyl-2*H*-tetrazolium bromide (MTT) and 4,6-diamidino-2-phenylindole (DAPI) were purchased from Beyotime Biotechnology Co., Ltd.

(Shanghai, China). D-Luciferin potassium salt was purchased from BioVision, Inc. (CA, USA). Anti-TGF- β antibody was purchased from Proteintech Group, Inc. (IL, USA). Anti-CD62P antibody, anti-CD31 antibody and anti-CD41 antibody were purchased from Abcam Co., Ltd. (Cambridge, UK). Anti-CD4 antibody, anti-FOXP3 antibody, anti-CD8a antibody, anti-IFN- γ antibody, anti-CD11c antibody, anti-CD80 antibody, anti-CD86 antibody, anti-CD11b antibody and anti-Ly6G antibody were purchased from eBioscience, Inc. (CA, USA).

2.2. Cell lines and animals

Mouse breast cancer cells (4T1) were purchased from the Shanghai Institutes for Biological Sciences (SIBS, Shanghai, China). And the 4T1-Luc cells were transfected with 4T1 cells in our lab. Both 4T1 cells and 4T1-Luc cells were cultured in RPMI 1640 medium (Gibco, CA, USA) at 37 °C with 5% CO₂. Culture medium was supplemented with 10% FBS (Gibco, CA, USA) and 1% Penicillin-Streptomycin Solution.

Female BALB/c mice (6–8 weeks) were purchased from Dashuo Experimental Animal Company (Chengdu, China). All animal experiments were conducted in accordance with the guidelines approved by Experimental Animals Administrative Committee of Sichuan University (Chengdu, China).

2.3. Preparation and characterization of micelles FD/DOX and DD/DOX

DOX-loaded micelles FD/DOX and DD/DOX were prepared as follows: Fu-DOCA or Dex-DOCA (10 mg) and DOX (0.5 mg) were dispersed in methanol (1 mL), the mixture was then added dropwise into 5% glucose (10 mL) with stirring. Thirty minutes later, the remained methanol was completely removed by rotary evaporation to obtain the DOX-loaded micelles. The particle size was measured by Dynamic Light Scattering (DLS; Malvern Instruments Co., Ltd., Zetasizer Nano ZS90, Worcestershire, UK), and the morphology was observed by Transmission Electron Microscope (TEM; JEOL, JEM-100CXII, Japan).

2.4. In vitro activated platelets binding test

Platelets collected from BALB/c mice were suspended gently in PBS (pH 7.4) for further use. Half of them were incubated with thrombin (1 U/mL) at 37 °C for 30 min for activation. Platelets with or without activation were then incubated separately with FD/DOX or DD/DOX at 37 °C. Twenty minutes later, the platelets were centrifuged (3500 rpm) for 10 min (Eppendorf Co., Ltd., 5415R, Hamburg, Germany) and resuspended in PBS (pH 7.4). The mean fluorescence was quantified by Flow Cytometer (Beckman Coulter, Inc., Cytomics FC 500, CA, USA), and the fluorescent images of platelets were photographed by Confocal Laser Scanning Microscope (CLSM; Olympus Co., Ltd., FV1000, Japan). To explore the mechanism of the binding between activated platelets and FD, activated platelets were pre-incubated with anti-CD62P antibody for 30 min before FD/DOX incubation. The mean fluorescence intensity was then quantified by Flow Cytometer (Beckman Coulter, Inc.).

2.5. Cellular uptake assay

4T1 cells were seeded into 6-well plates and incubated overnight. Next, the medium was replaced by fresh serum-free medium

containing DOX, DD/DOX or FD/DOX, respectively. After incubation for 1 or 4 h, the cells were stained with DAPI and observed by CLSM (Olympus Co., Ltd.). The mean fluorescence intensity of 4T1 cells was also quantified by Flow Cytometer (Beckman Coulter, Inc.).

To explore the mechanism of cellular uptake, 4T1 cells were pre-placed at 4 °C or pre-incubated with chlorpromazine, nystatin or amiloride for 30 min before incubating with DD/DOX or FD/DOX for another 4 h. The mean fluorescence intensity of 4T1 cells was finally quantified by the Flow Cytometer (Beckman Coulter, Inc.).

In order to explore the effect of platelet presence on cellular uptake, 4T1 cells were pre-incubated with activated platelets for 30 min before incubating with DD/DOX or FD/DOX for another 2 h. The 4T1 cells were then stained with DAPI and observed by CLSM (Olympus Co., Ltd.). The mean fluorescence intensity of 4T1 cells was also quantified by Flow Cytometer (Beckman Coulter, Inc.).

To track the intracellular delivery of FD/DOX and DD/DOX, 4T1 cells incubated with DD/DOX or FD/DOX were stained with Lyso-Tracker Red and DAPI, and then observed by CLSM (Olympus Co., Ltd.).

2.6. In vivo biodistribution

1×10^6 4T1 cells were inoculated on the back of female BALB/c mice to establish the 4T1 spontaneous metastasis model. On Days 10 and 30 after 4T1 cells inoculation, the mice ($n = 9$) were injected with DOX, DD/DOX or FD/DOX (DOX-equivalent 2.5 mg/kg) through tail vein, respectively. At 1, 8 and 24 h, 3 mice of each group were sacrificed, and the blood, tumors and major organs collected from mice were imaged by *In Vivo* Imaging System (IVIS; PerkinElmer, Inc., Lumina Series III, CA, USA). In addition, the sections of tumors, lungs and livers at 24 h were used to explore the distribution of different preparations. Platelets, neovasculature, and P-selectin were also stained in the sections.

The distribution of preparations in tumors and major organs at 24 h were further quantified by LC-MS (Agilent Technologies Co., Ltd., 6420 triple quadrupole, CA, USA) equipped with C18 column. Acetonitrile and 0.1% formic acid ($v/v = 28:72$) were used as mobile phase.

2.7. Anti-tumor and anti-metastasis assay on 4T1 spontaneous metastasis model

4T1 spontaneous metastasis model was established by 4T1-Luc cells as described before. After the inoculation of 4T1-Luc cells, the mice ($n = 15$) were injected with 5% Glu, Fu (50 mg/kg), DOX, DD/DOX or FD/DOX (DOX-equivalent 2.5 mg/kg) through tail vein, respectively, from Day 8. The preparations were administered every 3 days for a total of 7 times. Body weight and tumor volume were recorded during the treatment. In addition, luminescent signals of 4T1-Luc cells were monitored by IVIS (PerkinElmer, Inc.) every 7 days during the treatment.

On Day 35, 5 mice of each group were sacrificed to collected tumors and other major organs, and the remaining 10 mice of each group were used for the survival study. The obtained tumors were weighed and imaged, and the sections of tumor were applied for ki67 staining. The obtained lungs were photographed, and the metastatic nodules were counted carefully. Besides,

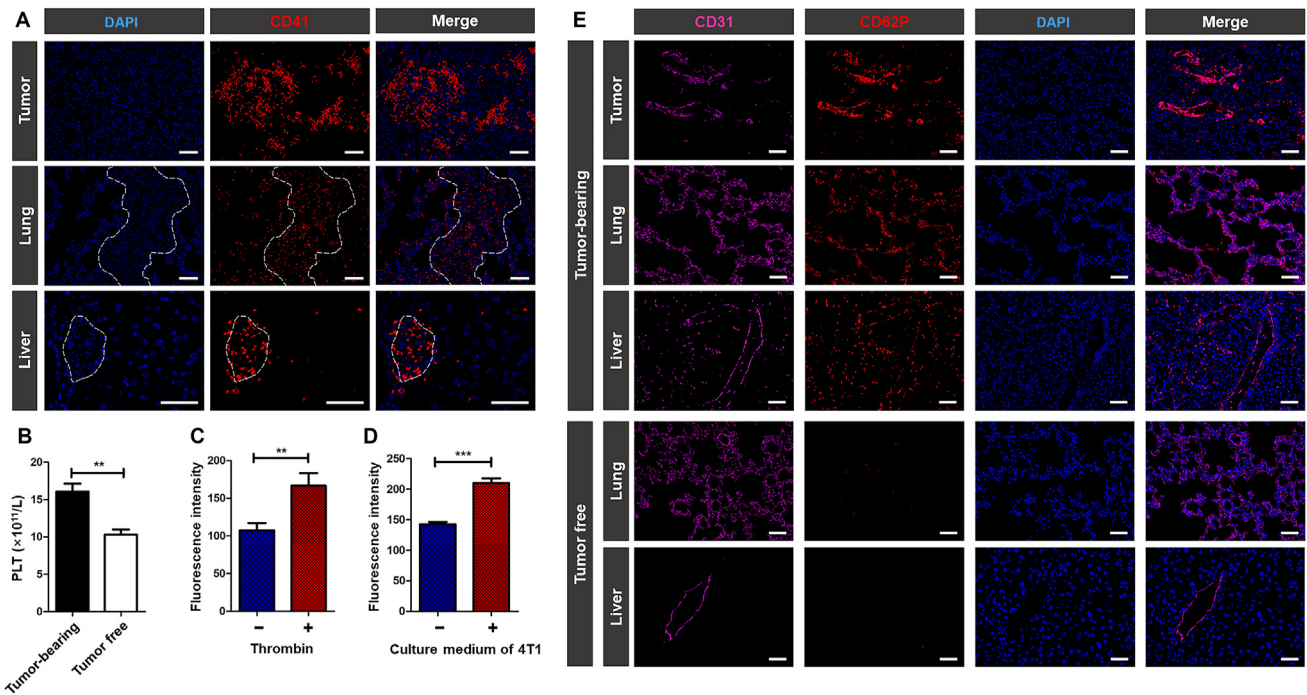


Figure 1 The distribution of platelets and the expression of P-selectin. (A) Fluorescent images of frozen sections of tumors, lungs and livers collected from 4T1 tumor-bearing mice. The area surrounded by white dotted lines represented metastasis in lungs and livers. Blue: DAPI for staining cell nucleus; red: CD41 for staining platelets. Scale bar = 100 μ m. (B) Count of the platelets in tumor free mice and 4T1 tumor-bearing mice. Data are presented as mean \pm SD ($n = 3$), ** $P < 0.01$. (C) Flow Cytometer detection of P-selectin expression on platelets with or without thrombin activation. Data are presented as mean \pm SD ($n = 3$), ** $P < 0.01$. (D) Flow Cytometer detection of P-selectin expression on HUVECs with or without the stimulation of 4T1 culture medium. Data are presented as mean \pm SD ($n = 3$), *** $P < 0.001$. (E) Fluorescent images of frozen sections of tumors, lungs and livers collected from 4T1 tumor-bearing mice and tumor free mice. Pink: CD31 for staining neovasculature; blue: CD62P for staining P-selectin; blue: DAPI for staining cell nucleus. Scale bar = 100 μ m.

all obtained tissues were stained with hematoxylin and eosin (H&E).

2.8. In vivo inhibition of TGF- β

As mentioned before, 4T1 tumor-bearing mice were injected with 5% Glu, Fu (50 mg/kg), DOX, DD/DOX or FD/DOX (DOX-equivalent 2.5 mg/kg) through tail vein, respectively, every 3 days for a total of 7 times. After the treatment, tumors, lungs and livers from mice were collected, and the sections of each tissue were applied for TGF- β staining. The TGF- β was also detected by Western blot assay. Tumors, lungs and livers from mice were collected and homogenized to collect proteins. The obtained proteins were first separated by acrylamide gel (12% SDS-PAGE). Next, the separated proteins were transferred to a polyvinylidene difluoride membrane. After that, the membrane was incubated with anti-TGF- β antibody and the secondary antibody in sequence. Finally, a Bioimage System (Bio-Rad Laboratories Inc., ChemiDoc MP, CA, USA) was used to measure the expression of TGF- β .

2.9. Detection of immune cells

The immune cells were quantitative detected by Flow Cytometer (Beckman Coulter, Inc.). As mentioned before, 4T1 tumor-bearing mice were injected with 5% Glu, DD/DOX or FD/DOX (DOX-equivalent 2.5 mg/kg) through tail vein, respectively, every 3 days for a total of 7 times. Then, mice were sacrificed on Day 7 after

the last dose. The tumors, spleens, livers and lungs were ground and filtered through cell strainers (70 μ m) to obtain cell suspension. The cells in spleen were stained with anti-CD11c antibody, anti-CD80 antibody and anti-CD86 antibody. The cells in tumor were stained with anti-CD4 antibody, anti-Foxp3 antibody, anti-CD-8a antibody and anti-IFN- γ antibody. Besides, the cells in lung and liver were stained with anti-CD11b antibody and anti-Ly6G antibody. The fluorescence was finally detected by the Flow Cytometer (Beckman Coulter, Inc.).

2.10. Statistical analysis

Data were shown as mean \pm standard deviations (SD). And the comparison between groups was performed by unpaired t -test. Significant differences between groups are represented by * $P < 0.05$, ** $P < 0.01$ and *** $P < 0.001$.

3. Result and discussion

Platelet plays a critical role in cancer development. The growing solid tumor can stimulate the production and activation of platelets, and the activated platelets will in turn promote tumor growth and metastasis³⁹. As shown in Fig. 1A and B, in 4T1 tumor-bearing mice, a large number of platelets were observed to be recruited to primary tumor and the metastatic site of lung and liver, and the platelet counts were higher than that of tumor free mice. The results

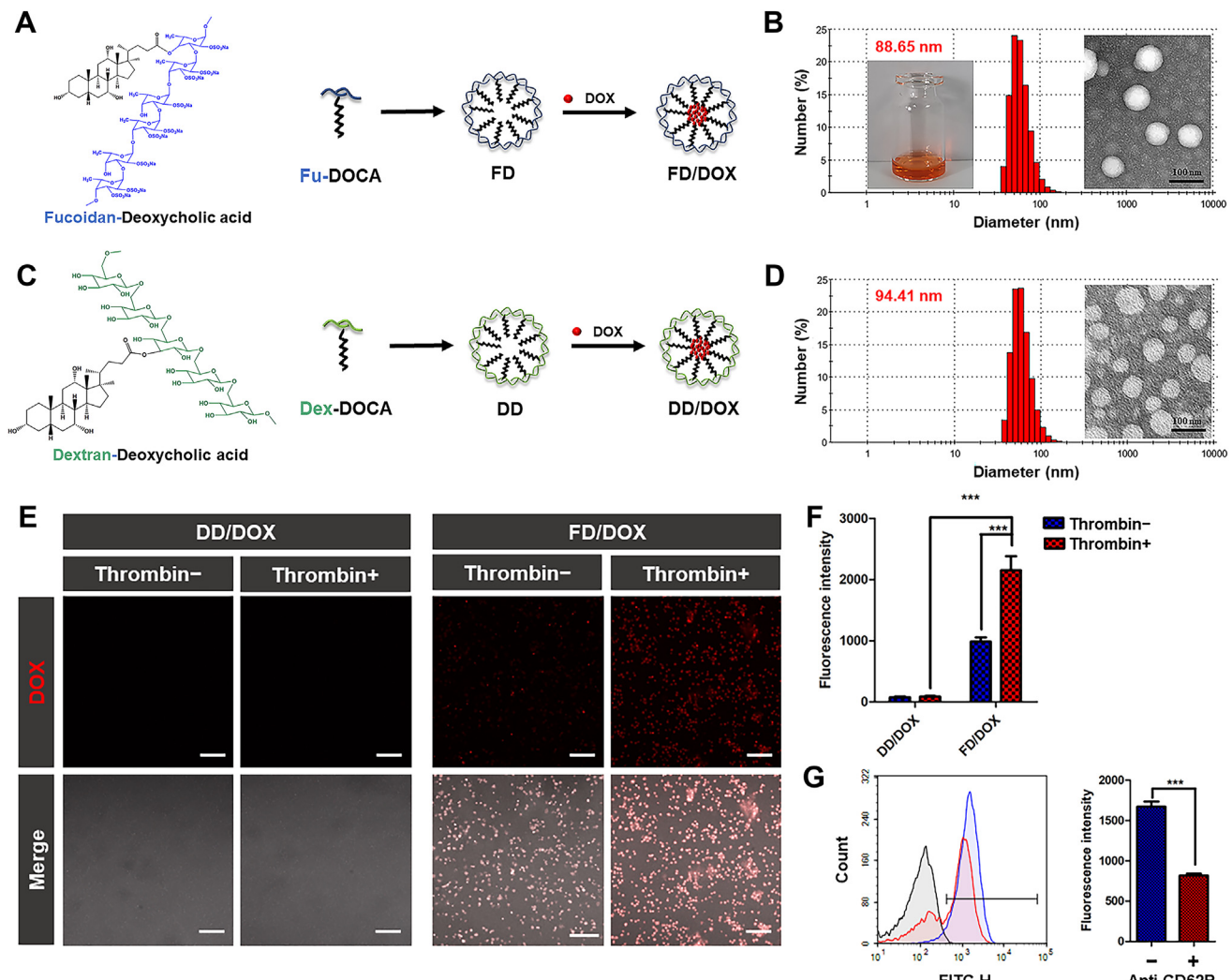


Figure 2 Characterization of micelles and activated platelets-binding ability. (A) The preparation of DOX-loaded micelle FD/DOX. (B) The appearance, TEM image and particle size distribution of FD/DOX. Scale bar = 100 nm. (C) The preparation of DOX-loaded micelle DD/DOX. (D) The TEM image and particle size distribution of DD/DOX. Scale bar = 100 nm. (E) Fluorescent images of platelets with or without activation incubated separately with FD/DOX and DD/DOX for 20 min. Scale bar = 100 μ m. (F) Flow Cytometer detection of the micelles bound to platelets with or without activation. Data are presented as mean \pm SD ($n = 3$), *** $P < 0.001$. (G) Flow Cytometer detection of FD/DOX bound to activated platelets with or without anti-CD62P antibody pre-incubation. Data are presented as mean \pm SD ($n = 3$), *** $P < 0.001$.

confirmed that tumor can promote platelet production, and the activated platelets had tumor and metastasis homing ability.

P-selectin is a glycoprotein overexpressed on activated platelets⁴⁰. As shown in Fig. 1C, *in vitro* detection suggested that platelets activated by thrombin exhibited higher expression of P-selectin. Therefore, P-selectin was considered as a potential target for activated platelets. Besides, various inflammatory factors secreted by tumor cells, such as TNF- α , can stimulate vascular endothelium to increase the expression of P-selectin⁴¹. As shown in Fig. 1D and Supporting Information Fig. S1, after incubating with the culture medium of 4T1 cells, HUVECs showed higher expression of P-selectin. And in Fig. 1E, the expression of P-selectin on vascular endothelium in primary tumor and around metastasis was significantly increased, facilitating the accumulation of P-selectin targeting nanoparticles in tumor and metastatic site.

3.1. Synthesis and characterization of Fu-DOCA and Dex-DOCA

Fucoidan is reported to exhibit nanomolar affinity for P-selectin^{30,31}. Therefore, in this study, the P-selectin targeting micelle specifically hitchhiking on activated platelets was constructed by fucoidan (Fu) and deoxycholic acid (DOCA). And the micelle constructed by dextran (Dex) and DOCA was used as a control without P-selectin targeting effect.

The amphiphilic polymer Fu-DOCA and Dex-DOCA were synthesized follow the route in Supporting Information Scheme S1. And the structures were characterized by ^1H NMR. As shown in Supporting Information Fig. S2, there were characteristic peaks of fucoidan (3.5–4.0 ppm) and DOCA (1.0–2.0 ppm) in the ^1H NMR spectrum of Fu-DOCA, while the peak of carboxyl (11.9 ppm) disappeared, indicating successful synthesis of Fu-

DOCA. Similarly, in *Supporting Information Fig. S3*, the characteristic peaks of dextran (3.0–4.0 ppm) and DOCA (1.0–2.0 ppm) were exhibited in the ^1H NMR spectrum of Dex-DOCA, the peak of carboxyl (11.9 ppm) disappeared, suggesting the successful synthesis of Dex-DOCA.

The structures of Fu-DOCA and Dex-DOCA were also characterized by IR. As shown in *Supporting Information Fig. S4*, characteristic peak at 1073 cm^{-1} was assigned to the sulfate groups of fucoidan, characteristic peaks at 3549 and 1715 cm^{-1} were attributed to the carbonyl group of DOCA. As for Fu-DOCA, the peaks at 1711 , 1090 , 1040 cm^{-1} and the disappeared peak at 3549 cm^{-1} confirmed the formation of ester bond between fucoidan and DOCA. In *Supporting Information Fig. S5*, dextran showed characteristic peaks at 2928 , 1644 and 995 cm^{-1} . As for Dex-DOCA, characteristic peaks of dextran still existed, the peak at 1736 cm^{-1} and the disappeared peak at 3550 cm^{-1} confirmed the formation of ester bond between dextran and DOCA.

3.2. Preparation and characterization of micelles FD, DD, FD/DOX and DD/DOX

The polymer Fu-DOCA and Dex-DOCA were self-assembled in 5% glucose (Glu) to prepare the micelles FD and DD (*Fig. 2A* and C). As shown in *Supporting Information Table S1* and *Fig. S6*, the obtained micelles had similar particle size (about 120 nm) and zeta potential (about -20 mV). In addition, the low CMC of FD ($7.38\text{ }\mu\text{g/mL}$) and DD ($10.99\text{ }\mu\text{g/mL}$) indicated that micelles could resist blood dilution and remain stable at low concentrations (*Supporting Information Fig. S7*). Hemolysis assay was used to investigate the interactions of micelles with blood erythrocytes. Image in *Supporting Information Fig. S8* shows the structure of blood erythrocytes had little change after incubating with FD. And in *Supporting Information Fig. S9*, hemolysis of FD and DD was calculated to be lower than 5% at different concentration (0.3, 0.5 and 1.0 mg/mL) within 8 h. These results suggest neither FD nor DD had hemolysis side-effect. The preliminary stability of micelles was investigated in 10% FBS or 50% FBS. As shown in *Supporting Information Fig. S10*, both FD and DD remained stable within 24 h, the particle size and the transmittance did not change obviously.

The hydrophobic DOX was encapsulated in the micelles to prepare FD/DOX and DD/DOX (*Fig. 2A* and C). As shown in *Table S1*, *Fig. 2B* and D, the DOX-loaded micelles were spherical with uniform size distribution. Both FD/DOX and DD/DOX had similar particle size (about 90 nm) and zeta potential (about -20 mV). The particle size and PDI of micelles loaded with DOX were smaller than that of blank micelles. The changes in size and dispersibility might be caused by the interaction between DOX and hydrophobic segment DOCA.

The release of DOX from micelles was investigated in PBS (pH 7.4, 6.5 and 5.0). In this study, polymer Fu-DOCA and Dex-DOCA was connected through ester bond, which would break in an acidic environment. As shown in *Supporting Information Fig. S11*, DOX in FD/DOX and DD/DOX had similar release behavior. In pH 7.4 PBS, the accumulative release of DOX within 36 h was less than 20%, indicating the micelles could remain stable in physiological environment. In pH 6.5 PBS, the accumulative release of DOX within 12 h was about 30%, while it increased to about 80% in pH 5.0 PBS. The results suggested that the release of DOX from FD/DOX and DD/DOX was acid-dependent, and DOX could be released quickly in the acidic lysosomal environment after cellular uptake.

3.3. FD/DOX efficiently bound to activated platelets via P-selectin

Activated platelets binding ability was an important characteristic of micelles in this study. To verify the adhesion between FD and activated platelets, platelets were isolated from BALB/c mice, and half of them were activated by thrombin. Platelets with or without thrombin activation were then incubated with FD/DOX at $37\text{ }^\circ\text{C}$ for 20 min. The DD/DOX was served as a control. As demonstrated in fluorescent images (*Fig. 2E*), there was significantly stronger fluorescence of the activated platelets incubated with FD/DOX than that incubated with DD/DOX. And after the FD/DOX incubation, there was more fluorescence on activated platelets than that on platelets without activation. In *Fig. 2F*, the fluorescence quantified by Flow Cytometer (Beckman Coulter, Inc.) also shows similar results. These results demonstrate that FD/DOX could efficiently bind activated platelets.

In order to verify that FD/DOX bound to activated platelets *via* P-selectin, half of the activated platelets were pre-incubated with anti-CD62P antibody before incubating with FD/DOX. As shown in *Fig. 2G*, the fluorescence quantified by Flow Cytometer (Beckman Coulter, Inc.) was obviously weakened when pre-treated with the anti-CD62P antibody, which demonstrated that FD/DOX specifically bound to P-selectin on activated platelets.

3.4. Increased cellular uptake efficiency and cytotoxicity of FD/DOX

Cellular uptake assay was conducted on 4T1 cells. As shown in fluorescent images (*Fig. 3A*), after incubation for 1 or 4 h, there was significantly higher cellular uptake of FD/DOX than that of DD/DOX and free DOX. In *Fig. 3B*, the fluorescence analyzed by Flow Cytometer (Beckman Coulter, Inc.) also shows similar result, suggesting that FD/DOX could be internalized quickly and efficiently. In order to explore the mechanism of cellular uptake, 4T1 cells were pre-placed at $4\text{ }^\circ\text{C}$ or pre-incubated with chlorpromazine (clathrin-dependent endocytosis inhibitor), nystatin (lipid raft-dependent endocytosis inhibitor) or amiloride (micro-pinocytosis inhibitor) for 1 h before incubating with DD/DOX or FD/DOX⁴². As shown in *Supporting Information Fig. S12*, the uptake of FD/DOX was inhibited by low temperature and various inhibitors, indicating multiple uptake mechanisms were involved, which might lead to the increased cellular uptake of FD/DOX.

Activated platelets was reported to adhere to CTCs as “protective coats” to guard the cells from elimination, and promote the development of cancer¹². Therefore, it was important to explore the cellular uptake of micelles in the presence of activated platelets. 4T1 cells were pre-incubated with activated platelets for 30 min before incubating with DD/DOX or FD/DOX. As shown in fluorescent images (*Fig. 3C*), the cellular uptake of DD/DOX was significantly reduced when pre-incubated with activated platelets, since the adhesion of platelets to the surface of 4T1 cells would prevent tumor cells from contacting DD/DOX. However, the cellular uptake of FD/DOX was increased when pre-incubated with activated platelets. In *Fig. 3D*, the fluorescence analyzed by Flow Cytometer (Beckman Coulter, Inc.) also shows similar result, suggesting that the activated platelets-adhering micelle FD/DOX could be internalized more efficiently by 4T1 cells, even in the presence of platelets. This phenomenon might be because the activated platelets can act as a “bridge” between FD/DOX and tumor cells, thereby increasing the contact of FD/DOX with 4T1 cells.

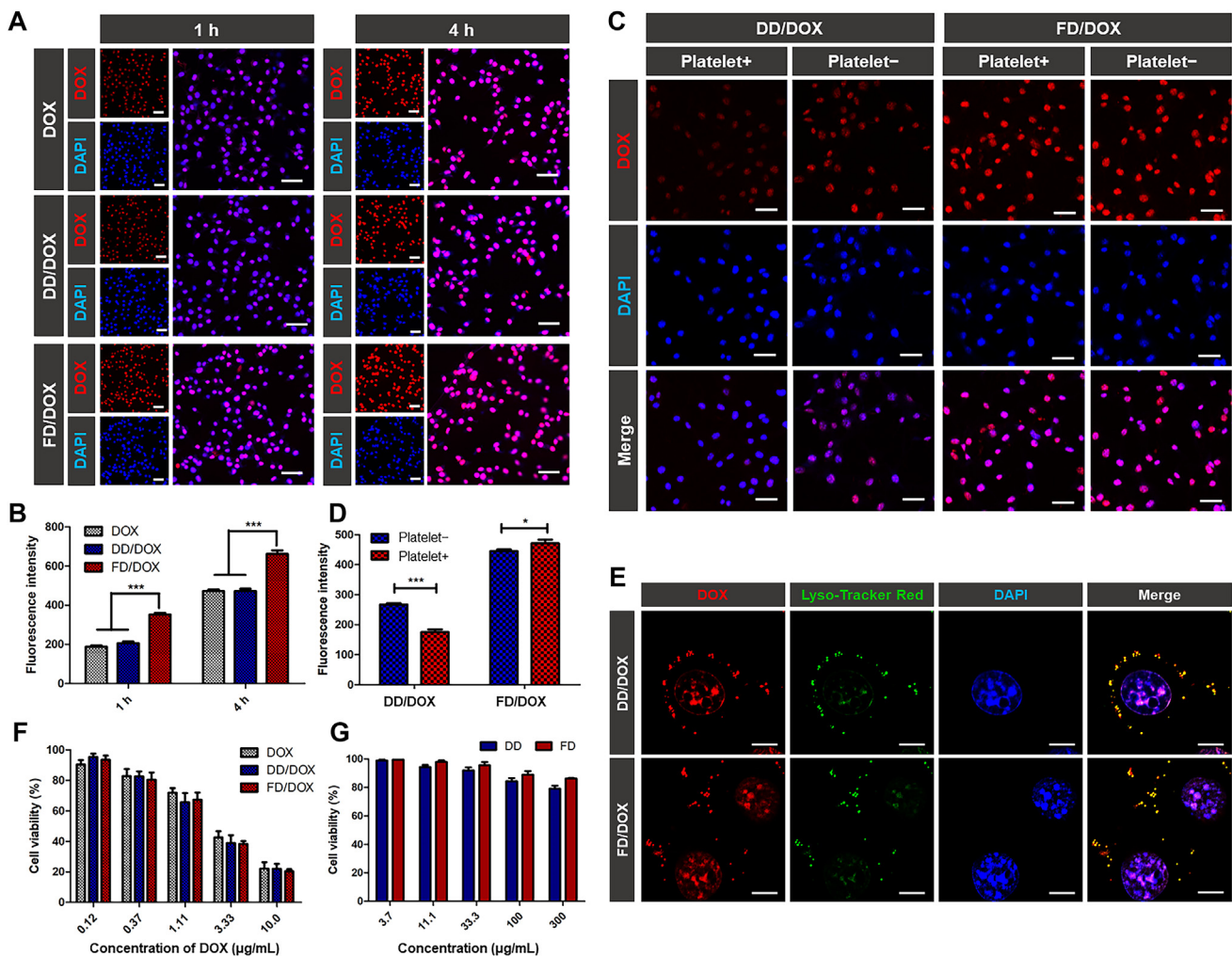


Figure 3 Cellular uptake efficiency and cytotoxicity of preparations on 4T1 cells. (A) Fluorescent images of 4T1 cells after incubating with free DOX, DD/DOX or FD/DOX, respectively, for 1 or 4 h. Red: DOX; blue: DAPI for staining cell nucleus. Scale bar = 100 μm. (B) Flow Cytometer detection of cellular uptake after incubating with free DOX, DD/DOX or FD/DOX, respectively, for 1 or 4 h. Data are presented as mean ± SD ($n = 3$), *** $P < 0.001$. (C) Fluorescent images of 4T1 cells after incubating with DD/DOX or FD/DOX, respectively, with or without the activated platelet pre-incubation. Red: DOX; blue: DAPI for staining cell nucleus. Scale bar = 100 μm. (D) Flow Cytometer detection of cellular uptake after incubating with DD/DOX or FD/DOX, respectively, with or without the activated platelet pre-incubation. Data are presented as mean ± SD ($n = 3$), * $P < 0.05$, *** $P < 0.001$. (E) Fluorescent images of 4T1 cells after incubating with DD/DOX or FD/DOX, respectively, for 1 h. Red: DOX; green: Lyso-Tracker Red for staining lysosome; blue: DAPI for staining cell nucleus. Scale bar = 10 μm. (F) Cell viability after incubating with DOX, DD/DOX or FD/DOX, respectively, for 24 h. Data are presented as mean ± SD ($n = 3$). (G) Cell viability after incubating with DD or FD, respectively, for 24 h. Data are presented as mean ± SD ($n = 3$).

In addition, to track the intracellular behavior of the micelles, lysosomes were stained with Lysotracker Red. As shown in fluorescent images (Fig. 3E), the micelles and lysosomes showed obvious co-localization, which indicated both DD/DOX and FD/DOX could reach lysosomes after cellular uptake. And the fluorescence signal of DOX in nucleus suggested that DOX was released from the micelles in an acidic lysosomal environment and entered the nucleus successfully.

The cytotoxicity evaluation was conducted on 4T1 cells. In Fig. 3F, DOX-loaded micelles DD/DOX and FD/DOX showed concentration-dependent cytotoxicity, and there was no significant difference compared to DOX. While in Fig. 3G, DD and FD didn't significantly affect cell viability even at 300 μg/mL, suggesting blank micelles DD and FD had almost no cytotoxicity on 4T1 cells.

3.5. Prolonged circulation time of FD/DOX

Platelets were inherent components of blood circulation and had relatively long lifetime; thus FD/DOX might have long circulation time by hitchhiking on platelets. In this study, the pharmacokinetics assay was performed in BALB/c mice. Plasma was collected at predetermined time points after intravenous injection of free DOX, DD/DOX or FD/DOX (DOX-equivalent 2.5 mg/kg). The drug concentration–time curve is shown in Supporting Information Fig. S13. And the pharmacokinetic parameters in Supporting Information Table S2 suggest that the area under the curve $AUC_{0-\infty}$ of FD/DOX (1757.475 μg h/L) was higher than that of DD/DOX (1218.591 μg h/L) and free DOX (649.682 μg h/L), and the $t_{1/2}$ of free DOX (0.932 h) was prolonged by DD/DOX (4.434 h).

and FD/DOX (6.35 h). These results prove FD/DOX exhibited longer circulation lifetime than DD/DOX by hitchhiking on platelets.

3.6. Enhanced targeting ability of FD/DOX to primary tumor and metastasis

The accumulation of nanoparticles in tumor is critical for its anti-tumor efficacy. However, the removal of nanoparticles by the reticuloendothelial system (RES) usually leads to a lack of anti-tumor efficacy, since only a small portion of nanoparticles can reach the tumor site.⁴³ In this study, the biodistribution of micelles was investigated at different stages of cancer.

On Day 10 after 4T1 cells inoculation, the early stage of cancer development, mice were intravenously injected with DOX, DD/

DOX or FD/DOX (DOX-equivalent 2.5 mg/kg), respectively, and sacrificed at 1, 8 and 24 h. The time-dependent biodistribution of DOX, DD/DOX and FD/DOX measured by IVIS (PerkinElmer, Inc.) was shown in Fig. 4A. The semiquantitative analysis of mean fluorescence intensity of tumors and major organs was shown in Fig. 4B and Supporting Information Fig. S14. Free DOX was distributed mainly in the liver and kidney and cleared quickly. Compared with free DOX, DD/DOX showed stronger fluorescence signal in tumor because of the passive targeting effect. However, the fluorescence of DD/DOX in liver and kidney remained at a high level. As for FD/DOX, the fluorescence signal in tumor was strong at each time point, even stronger than that of DD/DOX, suggesting that FD/DOX could effectively accumulate in tumor for a long time. More importantly, FD/DOX showed obviously less

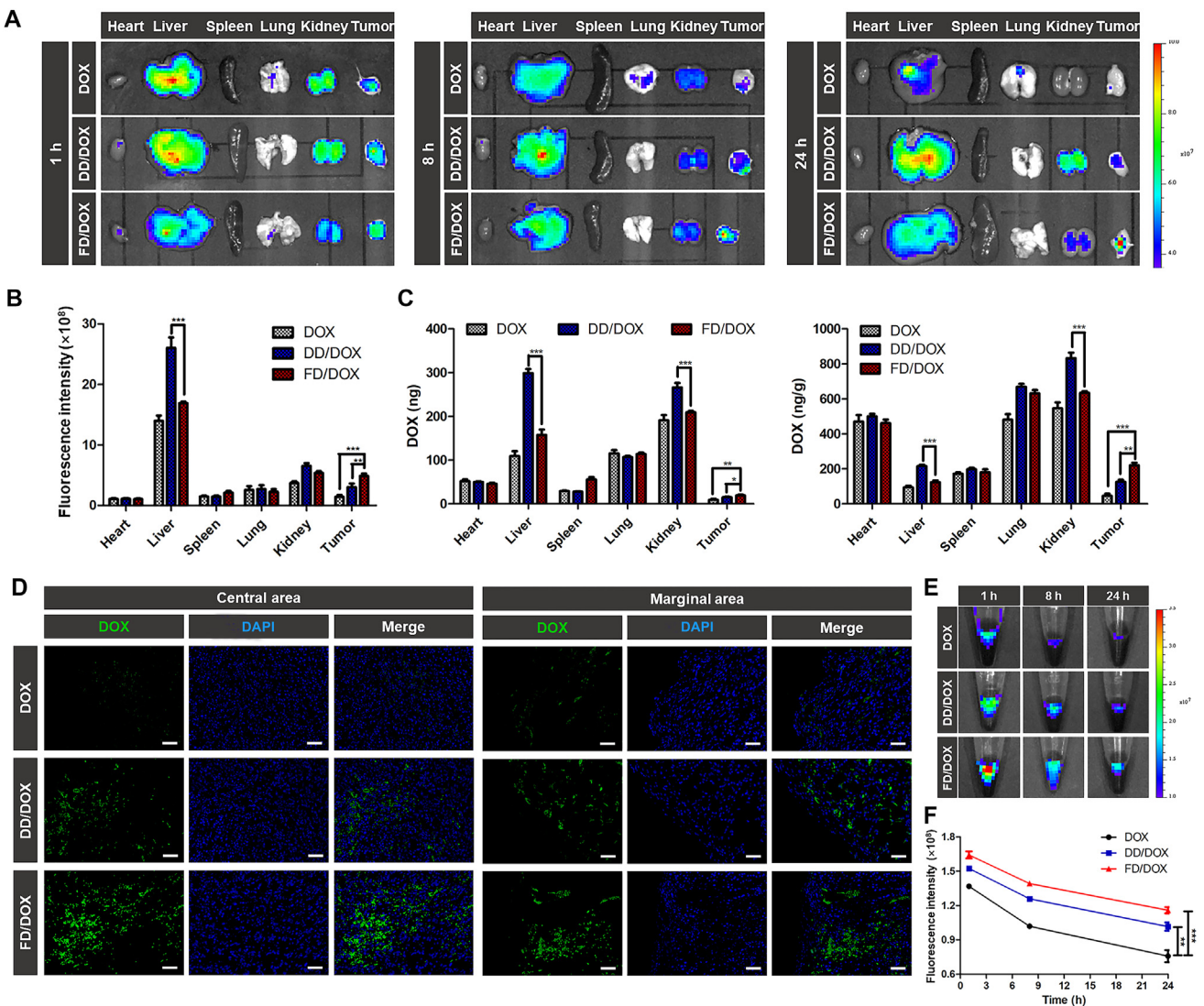


Figure 4 Biodistribution on Day 10 after 4T1 cells inoculation and tumor targeting capacity of different preparations. (A) Fluorescent images of tumors and major organs at 1, 8, 24 h after the administration of DOX, DD/DOX or FD/DOX. (B) Semiquantitative analysis of mean fluorescence intensity of tissues at 24 h after the administration. Data are presented as mean \pm SD ($n = 3$), ** $P < 0.01$, *** $P < 0.001$. (C) The amount of DOX in tumors and major organs quantified by LC-MS at 24 h after the administration. Data are presented as mean \pm SD ($n = 3$), * $P < 0.05$, ** $P < 0.01$, *** $P < 0.001$. (D) Fluorescent images of tumor sections at 24 h after the administration. Green: DOX; blue: DAPI for staining cell nucleus. Scale bar = 100 μ m. (E) Fluorescent images of blood collected from tumor-bearing mice at 1, 8, 24 h after the administration. (F) Semiquantitative analysis of mean fluorescence intensity of blood at 1, 8, 24 h after the administration. Data are presented as mean \pm SD ($n = 3$), ** $P < 0.01$, *** $P < 0.001$.

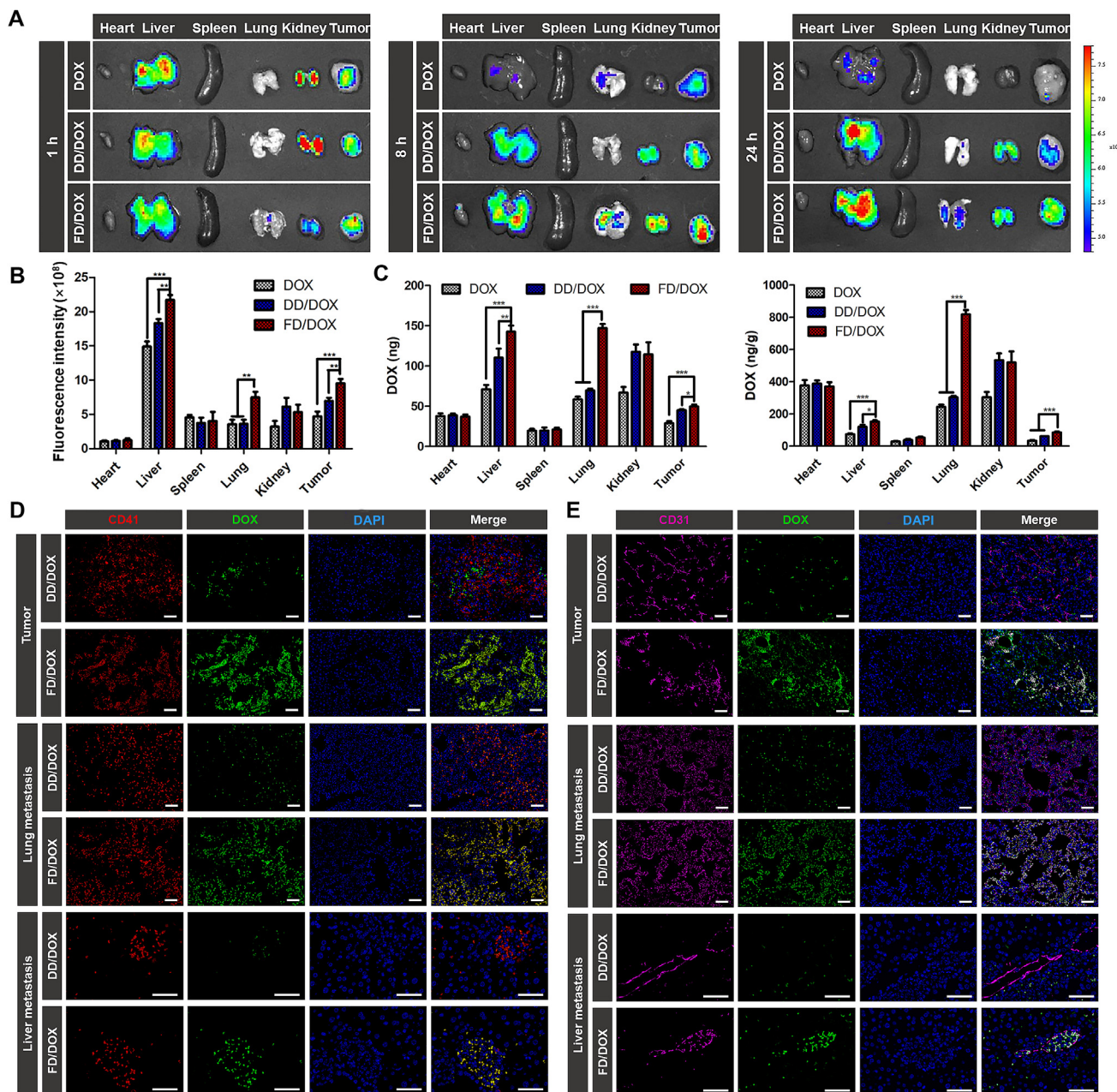


Figure 5 Biodistribution on Day 30 after 4T1 cells inoculation and metastasis targeting capacity of different preparations. (A) Fluorescent images of tumors and major organs at 1, 8, 24 h after the administration of DOX, DD/DOX or FD/DOX. (B) Semiquantitative analysis of mean fluorescence intensity of tissues at 24 h after the administration. Data are presented as mean \pm SD ($n = 3$), ** $P < 0.01$, *** $P < 0.001$. (C) The amount of DOX in tumors and major organs quantified by LC–MS at 24 h after the administration. Data are presented as mean \pm SD ($n = 3$), * $P < 0.05$, ** $P < 0.01$, *** $P < 0.001$. (D) Fluorescent images of frozen sections of tumor, lung metastasis and liver metastasis at 24 h after administration. Green: DOX; red: CD41 for staining platelets; blue: DAPI for staining cell nucleus. Scale bar = 100 μ m. (E) Fluorescent images of frozen sections of tumor, lung metastasis and liver metastasis at 24 h after administration. Green: DOX; pink: CD31 for staining neovasculature; blue: DAPI for staining cell nucleus. Scale bar = 100 μ m.

distribution in liver and kidney. In Fig. 4C, the biodistribution at 24 h quantitatively analyzed by LC–MS (Agilent Technologies Co., Ltd.) also shows the similar results. The fluorescent images of tumor sections at 24 h (Fig. 4D) further confirmed the distribution of FD/DOX was more than that of free DOX and DD/DOX in both central and marginal area. These results indicated that the micelle

FD/DOX hitchhiking on activated platelets had excellent tumor-targeting effect. And the reduced clearance of FD/DOX by RES might be owing to the masking effect of platelets.

Rapid circulatory clearance is also a major limitation in the development of nanoparticles. Herein, in Fig. 4E, the blood obtained from mice at 1, 8 and 24 h after administration was imaged

using IVIS (PerkinElmer, Inc.), and the semiquantitative analysis of mean fluorescence intensity was shown in Fig. 4F. At each time point, there was obviously higher fluorescence intensity of FD/DOX in blood than that of free DOX and DD/DOX, indicating FD/DOX had longer circulation lifetime in blood.

On Day 30 after 4T1 cells inoculation, the advanced stage of cancer development, metastasis had already appeared in lung and liver. The mice were intravenously injected with DOX, DD/DOX or FD/DOX as before, and sacrificed at 1, 8 and 24 h. As shown in Fig. 5A, the time-dependent biodistribution was measured by IVIS (PerkinElmer, Inc.). And the semiquantitative analysis of mean fluorescence intensity was shown in Fig. 5B and Supporting Information Fig. S15. Free DOX was cleared quickly, and there was almost no fluorescence signal at 24 h. The fluorescence of DD/DOX was strong in tumor, liver and kidney, while it was weak in the lung. As for FD/DOX, the fluorescence signal in tumor was stronger than that of free DOX and DD/DOX. In addition, compared with Day 10 after 4T1 cells inoculation, the distribution of FD/DOX in liver and lung was significantly increased. In Fig. 5C, the biodistribution at 24 h quantitatively analyzed by LC-MS (Agilent Technologies Co., Ltd.) also shows the similar results. The distribution of FD/DOX in the liver was about 1.5 times that of DD/DOX, and the distribution of FD/DOX in lungs was more than twice that of DD/DOX. These results suggest that the micelle FD/DOX had excellent metastasis-targeting effect.

The sections of tumors, lungs and livers were used to further explore the distribution of micelles. As confirmed before, a large number of platelets could be recruited to the primary tumor and metastatic site. To investigate whether the FD/DOX could bind platelets *in vivo*, platelets were stained with anti-CD41 antibody in the sections of tumors, lungs and livers. In Fig. 5D, the co-localization of CD41 and FD/DOX was observed in tumor and the metastasis, suggesting that FD/DOX could bind platelets effectively, thus exhibiting increased targeting effect on tumor and metastasis via “platelet bridge”. Neovasculature were also stained in the sections with anti-CD31 antibody. As shown in Fig. 5E, co-localization of CD31 and FD/DOX was observed, indicating that FD/DOX was able to bind neovasculature in tumor and the metastasis. And FD/DOX showed increased distribution around neovasculature, indicating enhanced penetrating ability. Therefore, FD/DOX exhibited excellent targeting ability on tumor and metastasis by simultaneously hitchhiking on activated platelets and adhering to neovasculature, which was actually due to its excellent P-selectin binding ability (Supporting Information Fig. S16).

3.7. Preliminary safety evaluation

The toxicity of preparations was evaluated by biochemical analysis and hematological analysis. BALB/c mice were intravenously injected with Glu, DOX, DD/DOX or FD/DOX (DOX-equivalent 2.5 mg/kg), respectively, every 3 days for a total of 7 times. As shown in Supporting Information Fig. S17, DOX injection decreased the number of lymphocytes and white blood cells, indicating DOX at this dosage might cause bone marrow toxicity. However, DD/DOX and FD/DOX injection did not exhibit obvious side effect, which suggested the micelles DD/DOX and FD/DOX would decrease the toxicity of DOX. In addition, Biochemical analysis showed no abnormalities. The preliminary safety evaluation demonstrated that both DD/DOX and FD/DOX was safe for injection.

3.8. Anti-tumor and anti-metastasis efficacy on 4T1 spontaneous metastasis model

4T1 spontaneous metastasis model was established by 4T1-Luc cells to investigate the *in vivo* anti-tumor and anti-metastasis efficacy. As shown in Fig. 6A, after 4T1-Luc cells inoculation, the mice were intravenously injected with Glu, Fu, DOX, DD/DOX or FD/DOX (DOX-equivalent 2.5 mg/kg), respectively, on Days 8, 11, 14, 17, 20, 23 and 26. Body weights of mice were recorded during the treatment (Supporting Information Fig. S18). As shown in Fig. 6B, the luminescent signals of 4T1-Luc cells were monitored on Days 19, 26 and 33 using IVIS (PerkinElmer, Inc.). And the semi-quantitative results of bioluminescence signals on Day 33 was shown in Fig. 6C and D. Compared with the other groups, the luminescent signal in tumor region of mice treated with FD/DOX was significantly reduced, indicating a strong inhibitory effect on 4T1 tumor. In addition, the luminescent signal in the lung area of mice treated with DOX and DD/DOX, was much stronger than that of mice treated with Fu, while there was almost no luminescent signal in the lung area of mice treated with FD/DOX. The results suggested that FD/DOX exhibited the most excellent inhibitory effect on metastasis.

The survival time of mice is influenced by both tumor volume and tumor metastasis, and metastasis is the most common cause of cancer death. Therefore, as shown in Fig. 6E, large tumor volume and severe metastasis together led to the death of the mice treated with DOX and DD/DOX. Fu had inhibitory effect on the metastasis, and thus mice treated with Fu had slightly longer survival time. And FD/DOX treatment significantly prolonged the survival time of 4T1 tumor-bearing mice due to its excellent anti-tumor and anti-metastasis efficacy.

In order to further assess the anti-tumor and anti-metastasis effects, mice were sacrificed at Day 35 to collected tumors and other major organs. The obtained tumors were weighed and imaged. As shown in Fig. 7A-C, free DOX and DD/DOX exhibited inhibitory effect on tumor in early stage, while the tumor volume increased rapidly after the last administration. However, both the volume and weight of tumors collected from FD/DOX treated mice were the smallest, and the tumor volume did not increase obviously after the last treatment, suggesting FD/DOX exhibited more excellent antitumor efficiency than other preparations. In addition, the tumor sections were applied for H&E staining and ki67 staining. As shown in Fig. 7D, the most extensive tissue necrosis and significantly reduced proliferation activity were observed in tumor treated with FD/DOX.

The anti-metastasis activity of preparations was evaluated in lung and liver, respectively. The obtained lungs were photographed, and the metastatic nodules on lungs were then counted carefully. As shown in Fig. 7E and F, a lot of metastasis nodules were observed on the surface of lungs treated with Glu, DOX and DD/DOX, while the nodules were almost invisible on the lung treated with FD/DOX. In addition, the sections of lungs and livers were applied for H&E staining. As shown in Fig. 7G, FD/DOX was confirmed to exhibit strong inhibitory effect on both lung metastasis and liver micrometastasis, which might be attributed to the binding ability to activated platelets. By hitchhiking on activated platelets, FD/DOX could not only enhance the targeting effect on tumor and metastasis, but also hunt and kill CTCs in blood circulation. Fu also exhibited anti-metastasis effect, which might because the binding of fucoidan with P-selectin on the vascular endothelium could competitively inhibit

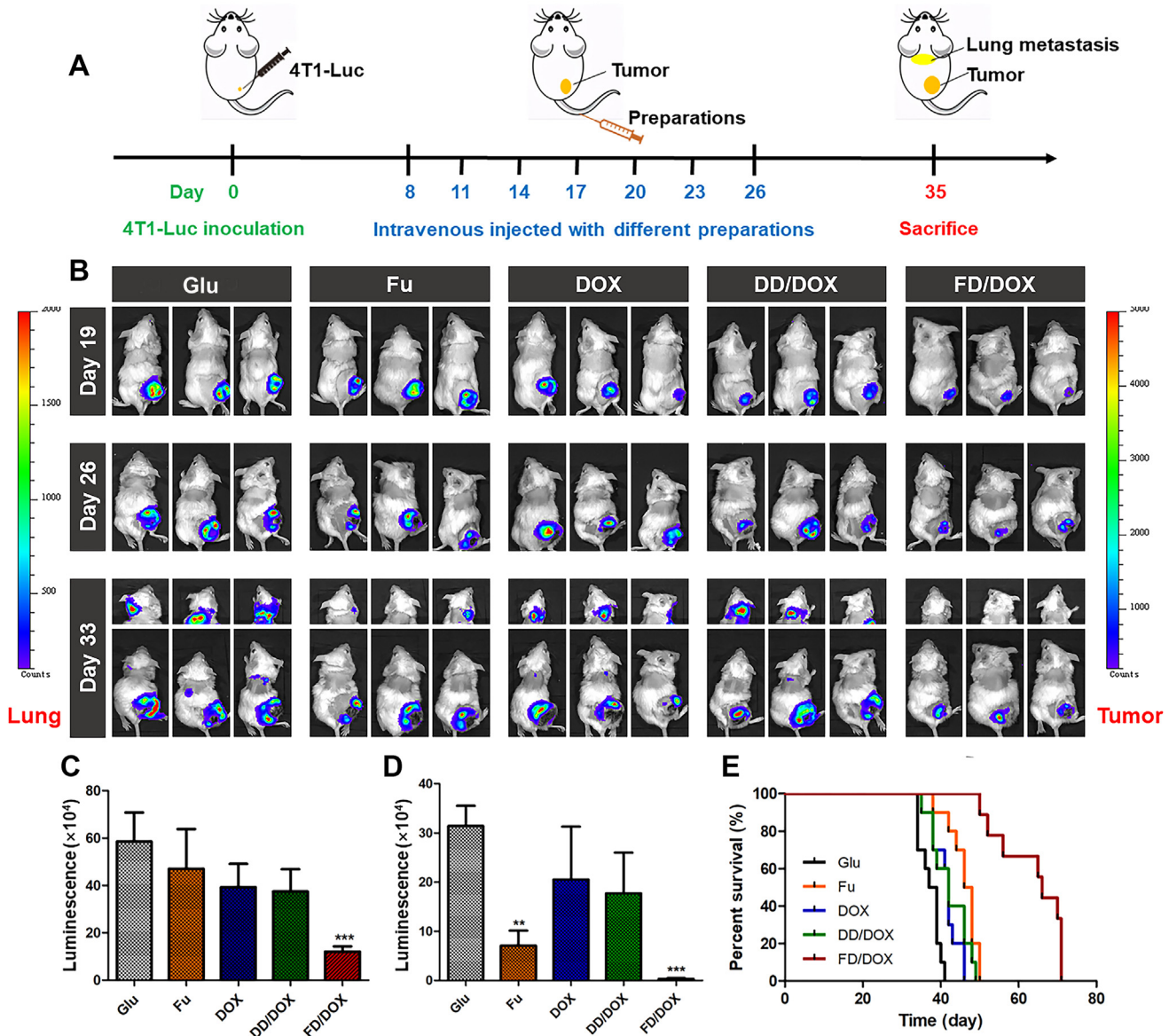


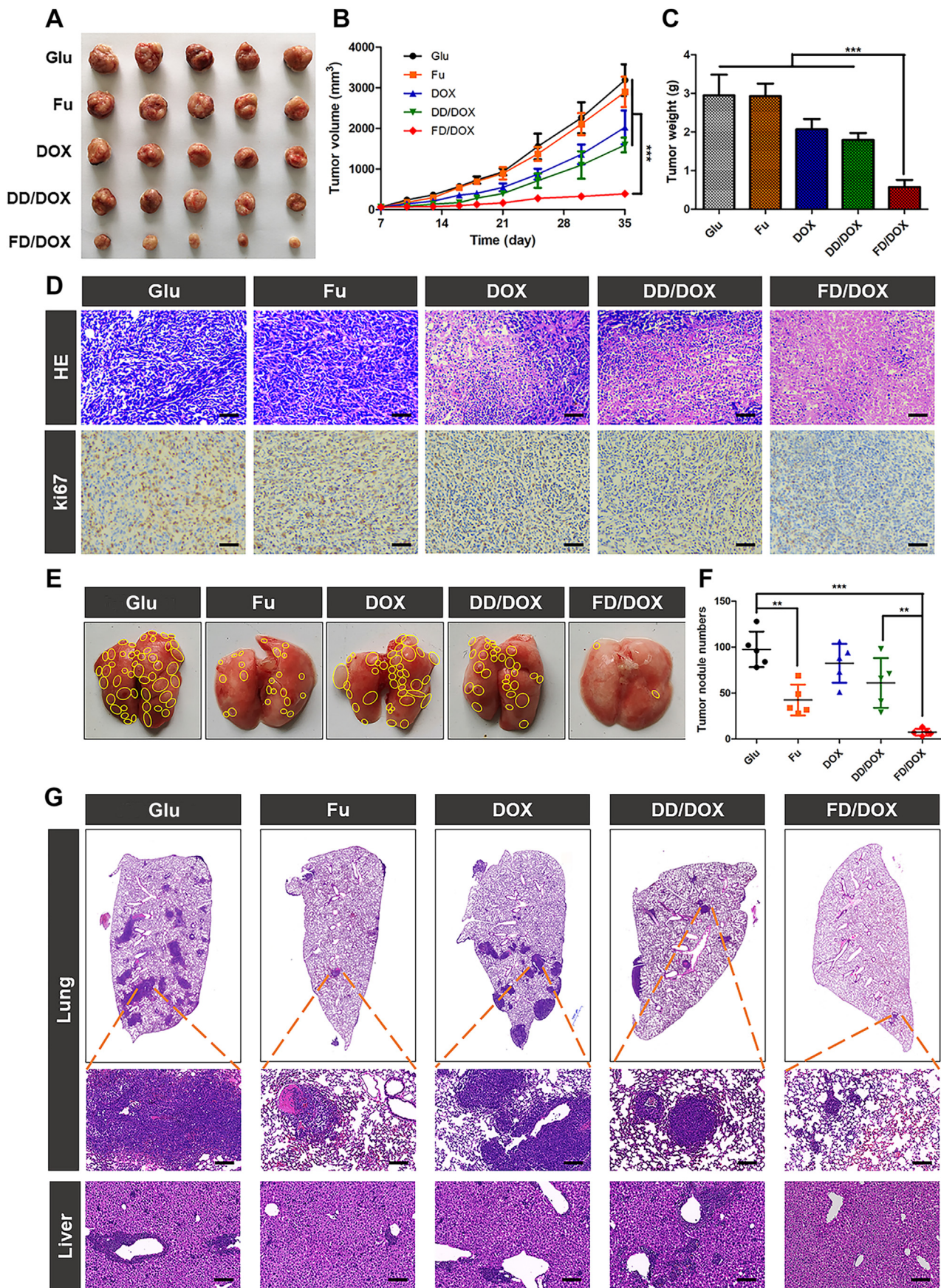
Figure 6 Anti-tumor and anti-metastasis effect on 4T1 spontaneous metastasis model. (A) The diagram of 4T1 spontaneous metastasis model and the treatment. (B) Bioluminescence imaging of tumors and lung metastasis in tumor-bearing mice treated with Glu, Fu, DOX, DD/DOX or FD/DOX (DOX-equivalent 2.5 mg/kg), respectively ($n = 3$). (C) Semi-quantitative analysis of bioluminescence signal of tumor. Data are presented as mean \pm SD ($n = 3$), *** $P < 0.001$. (D) Semi-quantitative analysis of bioluminescence signal of lung metastasis. Data are presented as mean \pm SD ($n = 3$), ** $P < 0.01$, *** $P < 0.001$. (E) Survival curve of 4T1 tumor-bearing mice treated with preparations ($n = 10$).

CTCs from adhering to vascular endothelium and implanting in distant organs.

In order to explore the long-time anti-metastasis effect of FD/DOX, on Day 47 after 4T1-Luc cells inoculation, that is, Day 20 after the last dose, the tumor-bearing mice in FD/DOX group were monitored using IVIS (PerkinElmer, Inc.). And the lungs and livers collected from the sacrificed mice were applied for H&E staining. As shown in Supporting Information Fig. S19A, after finishing the treatment for a period of time, the volume of solid tumor increased again, while there was still no obvious luminescent signal in the lung area of mice. And in Fig. S19B, the result of H&E staining also indicated there was no serious metastasis in lung and liver. Therefore, FD/DOX was considered to exist long-time anti-metastasis effect.

The spleens collected from mice were also imaged, and the sections of spleens were applied for H&E staining. As shown in Supporting Information Fig. S20, enlarged spleens with expanded red pulp and reduced white pulp were observed in 4T1 tumor-bearing mice. This phenomenon was documented in tumor-induced leukemoid reaction⁴⁴. As for mice treated with FD/DOX, compared with other groups, the volume of spleen was much smaller, and the H&E staining was observed similar with that of tumor free mice. This result was mainly due to the reduced tumor burden, which further confirmed the excellent inhibitory effect of FD/DOX on 4T1 tumor.

In addition, to evaluate the potential toxicity of preparations, the major organs of mice after treatment were collected for H&E staining. As shown in Supporting Information Fig. S21,



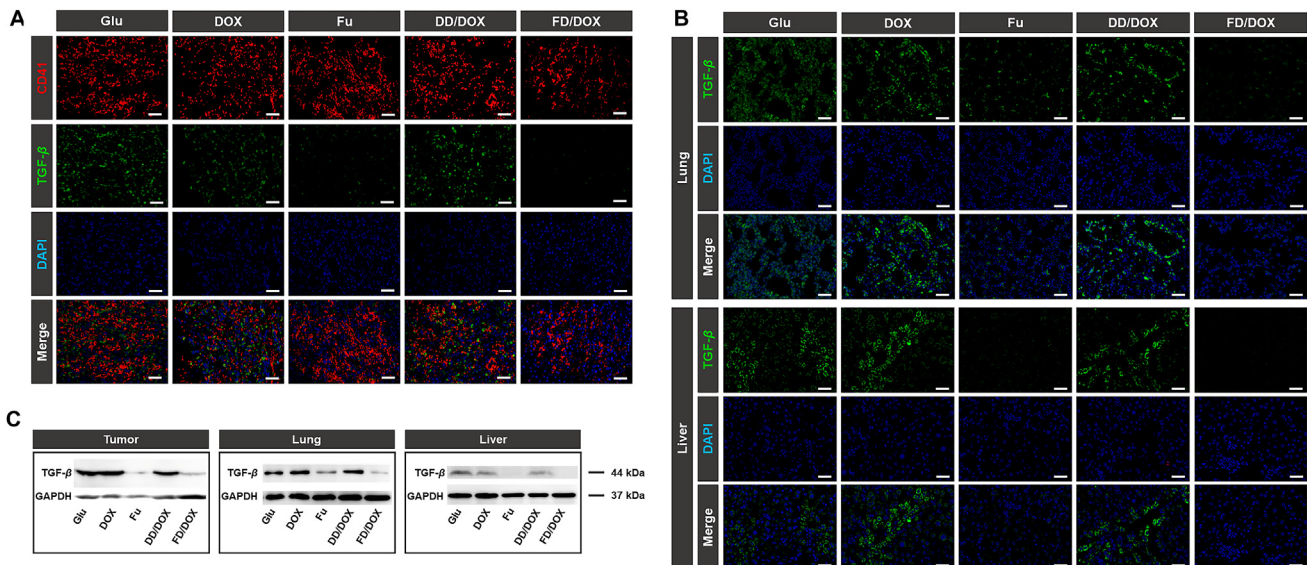


Figure 8 *In vivo* inhibition of TGF- β . (A) Fluorescent images of tumor sections treated with Glu, Fu, DOX, DD/DOX or FD/DOX (DOX-equivalent 2.5 mg/kg), respectively. Green: TGF- β ; blue: DAPI for staining cell nucleus; red: CD41 for staining platelets. Scale bar = 100 μ m. (B) Fluorescent images of frozen sections of lungs and livers collected from tumor-bearing mice after treatment. Green: TGF- β ; blue: DAPI for staining cell nucleus. Scale bar = 100 μ m. (C) Expression of TGF- β in tumors, lungs and livers detected by Western blot assay.

glomerular effusion was observed in DOX group. And there were no obvious morphological abnormalities found in other groups.

3.9. *In vivo* inhibition of TGF- β

TGF- β is an important component in tumor microenvironment which can induce epithelial-to-mesenchymal transition (EMT) of tumor cells²⁶. And in premetastatic organs, TGF- β is required for tumor cells colonization²⁷. Therefore, the inhibition of TGF- β in both primary tumor and premetastatic organs is necessary for effective cancer treatment. In this study, the activated platelets were confirmed to be recruited to primary tumor and metastasis, through which the micelle FD/DOX could track tumor cells accurately. However, the activated platelets also secreted TGF- β ¹¹, which was a serious problem of platelet-based therapy and remained to be solved.

Herein, the *in vivo* inhibitory effect on TGF- β was investigated on 4T1 tumor-bearing mice. The mice were intravenously injected with Glu, DOX, Fu, DD/DOX or FD/DOX, respectively, every 3 days for a total of 7 times. After that, tumors, lungs and livers were collected from mice and applied for TGF- β detection. As shown in Fig. 8A, high fluorescence signal of TGF- β was observed in tumor, especially at the site of platelets aggregation. And it was worth noting that FD/DOX treatment significantly decreased the fluorescence signal of TGF- β around platelets. The results suggested the micelle FD/DOX could inhibit TGF- β expression of activated platelets, and thus weakened the tumor promoting effect of tumor-homing platelets. In lung and liver, the

fluorescence signal of TGF- β was also reduced after Fu and FD/DOX treatment (Fig. 8B), which might remodel the environment for tumor cells colonization and finally lead to better anti-metastasis effect of FD/DOX. Besides, the expression of TGF- β in tumors, lungs and livers was also detected by immunohistochemical staining (Supporting Information Fig. S22) and Western blot assay (Fig. 8C and Supporting Information Fig. S23). The similar results confirmed the inhibitory effect of FD/DOX on TGF- β again. The inhibition of TGF- β was also observed in mice treated with Fu, indicating that the inhibitory effect of FD/DOX was actually attributed to fucoidan, the hydrophilic segment of micelle FD/DOX.

3.10. *In vivo* regulation of immune response

Fucoidan was reported to exhibit an immunostimulatory function³⁵. Therefore, the micelle FD/DOX might stimulate anti-tumor immune response effectively through the combination of fucoidan and DOX, a chemotherapy drug that cause immunogenic cell death of tumor cells. In addition, TGF- β is an immunosuppressive cytokine, which was reported to inhibit the maturation of dendritic cells (DCs) and the proliferation of CD4 $^{+}$ and CD8 $^{+}$ T cells²⁸. Therefore, the inhibition of TGF- β by FD/DOX might also enhance the anti-tumor immune response.

In order to verify the immunomodulatory effect, 4T1 tumor-bearing mice were intravenously injected with Glu, DD/DOX or FD/DOX (DOX-equivalent 2.5 mg/kg), respectively, every 3 days for a total of 7 times. On Day 7 after the last dose, the immune

Figure 7 Anti-tumor and anti-metastasis effect on 4T1 spontaneous metastasis model. (A) Image of 4T1 tumors treated with Glu, Fu, DOX, DD/DOX or FD/DOX (DOX-equivalent 2.5 mg/kg), respectively ($n = 5$). (B) The changes of tumor volume during treatment. Data are presented as mean \pm SD ($n = 5$), *** $P < 0.001$. (C) The weight of tumors after treatment. Data are presented as mean \pm SD ($n = 5$), *** $P < 0.001$. (D) H&E staining and ki67 staining for tumors. Scale bar = 100 μ m. (E) Images of lungs in different groups. The yellow circles represented metastatic nodules on lungs. (F) Count of metastatic nodules on lungs. Data are presented as mean \pm SD ($n = 5$), ** $P < 0.01$, *** $P < 0.001$. (G) H&E staining for lungs and livers, and the dark purple parts represented tumor metastasis. Scale bar = 100 μ m.

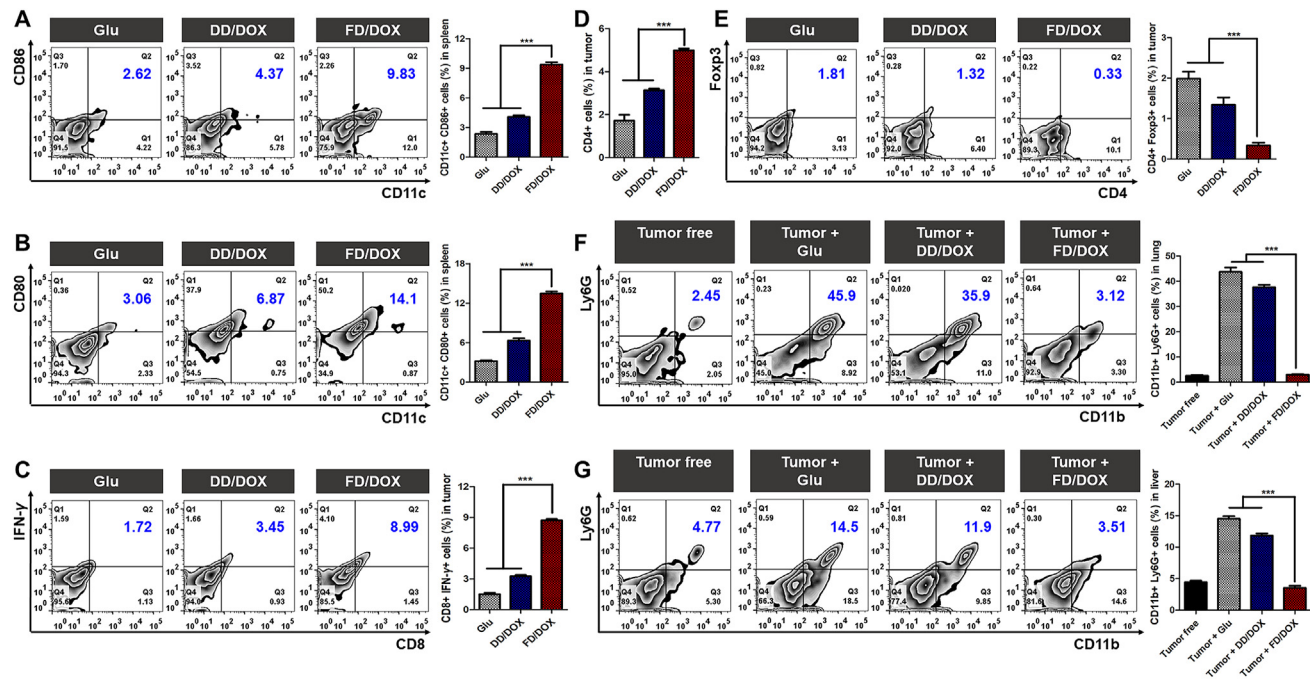


Figure 9 Immune cells of 4T1 tumor-bearing mice after treatment. Flow Cytometer detection and the percentages of (A) CD11c⁺ CD86⁺ cells in spleens, (B) CD11c⁺ CD80⁺ cells in spleens, (C) CD8⁺ IFN- γ ⁺ cells in tumors, (D) CD4⁺ cells in tumors, (E) CD4⁺ Foxp3⁺ cells in tumors, (F) CD11b⁺ Ly6G⁺ cells in lungs, and (G) CD11b⁺ Ly6G⁺ cells in livers. Data are presented as mean \pm SD ($n = 3$), *** $P < 0.001$.

cells were quantitative detected by Flow Cytometer (Beckman Coulter, Inc.). As shown in Fig. 9A and B, mature DCs (CD11c⁺ CD86⁺ cells and CD11c⁺ CD80⁺ cells) was significantly increased in spleens treated with FD/DOX. As in the 4T1 tumor, it was obvious that FD/DOX treatment enhanced the recruitment of CD8⁺ T cells (CD8⁺ IFN- γ ⁺ cells in Fig. 9C) and CD4⁺ T cells (CD4⁺ cells in Fig. 9D). Meanwhile, the immunosuppressive Tregs (CD4⁺ Foxp3⁺ cells in Fig. 9E) was decreased. These results demonstrate that FD/DOX exhibited strong immune stimulating effect, through which better anti-tumor efficacy could be achieved.

In addition, it was proved in many studies that the immunosuppressive G-MDSCs (CD11b⁺ Ly6G⁺ cells) can be recruited to distant organs and assist the formation of premetastatic niche (PMN), thus promoting the colonization and proliferation of tumor cells^{45,46}. As shown in Fig. 9F and G, the G-MDSCs in the lungs and livers of tumor-bearing mice were significantly more than that of tumor free mice. PSL-1 expressed on G-MDSCs was crucial for their recruitment by binding P-selectin on vascular endothelium⁴⁷. Therefore, the micelle FD/DOX might inhibit G-MDSCs recruitment in premetastatic organs by competitively binding P-selectin. The results in Fig. 9F and G confirm that FD/DOX treatment significantly reduced the percentage of G-MDSCs in the lungs and livers to a level similar to that in tumor free mice. The inhibition of G-MDSCs recruitment would further enhance CD8⁺ T cell-mediated immune response, since cytokines secreted by G-MDSCs, such as IL-10, could inhibit the activity of CD8⁺ T cells⁴⁸. As a result, FD/DOX treatment reversed the immunosuppressive microenvironment in distant organs, prevented the implantation and survival of tumor cells, and finally achieved better anti-metastasis efficacy.

4. Conclusions

In this study, a fucoidan-functionalized micelle FD/DOX was constructed successfully, which could adhere to activated platelets through P-selectin. The micelle FD/DOX could effectively target primary tumor, CTCs, and metastatic site in distant organs by hitchhiking on activated platelets recruited by tumor cells. P-selectin expressed on vascular endothelium also assisted the accumulation of FD/DOX. Accurately tracking and killing tumor cells resulted in excellent anti-tumor and anti-metastasis efficacy of FD/DOX. In addition, FD/DOX treatment was confirmed to inhibit the expression of TGF- β , which solved a trouble caused by platelet recruitment, and effectively stimulated anti-tumor immune response, contributing to the anti-cancer treatment. In summary, the fucoidan-functionalized activated platelets-targeting micelle provided a promising strategy for metastatic cancer treatment by accurately tracking of tumor cells and remodeling the microenvironment in primary tumor and premetastatic organs.

Acknowledgments

This work was supported by National Natural Science Foundation of China (81974499 and 81690261), and Sichuan Science and Technology Program (2018RZ0136).

Author contributions

Rong Guo and Qin He designed the research. Rong Guo and Miao Deng carried out the experiments and performed data analysis. Xuan He, Mengmeng Li, Jiaxin Li, Penghui He and Houqin Liu

participated part of the experiments. Zhirong Zhang provided some experimental instruments for this work. Rong Guo wrote the manuscript. Man Li and Qin He revised the manuscript. All of the authors have read and approved the final manuscript.

Conflicts of interest

The authors have no conflicts of interest to declare.

Appendix A. Supporting information

Supporting data to this article can be found online at <https://doi.org/10.1016/j.apsb.2021.05.012>.

References

- Steeg PS, Theodore D. Metastasis: a therapeutic target for cancer. *Nat Clin Pract Oncol* 2008;5:206–19.
- Klein CA. Parallel progression of primary tumours and metastases. *Nat Rev Canc* 2009;9:302–12.
- Mohme M, Riethdorf S, Pantel K. Circulating and disseminated tumour cells—mechanisms of immune surveillance and escape. *Nat Rev Clin Oncol* 2017;14:155–67.
- Gingis-Velitski S, Loven D, Benayoun L, Munster M, Bril R, Voloshin T, et al. Host response to short-term, single-agent chemotherapy induces matrix metalloproteinase-9 expression and accelerates metastasis in mice. *Cancer Res* 2011;71:6986–96.
- Ran S. The role of TLR4 in chemotherapy-driven metastasis. *Cancer Res* 2015;75:2405–10.
- Fidler IJ. The pathogenesis of cancer metastasis: the ‘seed and soil’ hypothesis revisited. *Nat Rev Cancer* 2003;3:453–8.
- Chaffer CL, Weinberg RA. A perspective on cancer cell metastasis. *Science* 2011;331:1559–64.
- Nguyen DX, Bos PD, Massagué J. Metastasis: from dissemination to organ-specific colonization. *Nat Rev Cancer* 2009;9:274–84.
- Franco AT, Corken A, Ware J. Platelets at the interface of thrombosis, inflammation, and cancer. *Blood* 2015;126:582–8.
- Xu XR, Yousef GM, Ni H. Cancer and platelet crosstalk: opportunities and challenges for aspirin and other anti-platelet agents. *Blood* 2018;131:1777–89.
- Haemmerle M, Stone RL, Menter DG, Afshar-Kharghan V, Sood AK. The platelet lifeline to cancer: challenges and opportunities. *Cancer Cell* 2018;33:965–83.
- Gay LJ, Felding-Habermann B. Contribution of platelets to tumour metastasis. *Nat Rev Cancer* 2011;11:123–34.
- Labelle M, Begum S, Hynes RO. Platelets guide the formation of early metastatic niches. *Proc Natl Acad Sci U S A* 2014;111:E3053–61.
- Lu Y, Hu Q, Jiang C, Gu Z. Platelet for drug delivery. *Curr Opin Biotechnol* 2019;58:81–91.
- Wang C, Sun W, Ye Y, Hu Q, Bomba HN, Gu Z. *In situ* activation of platelets with checkpoint inhibitors for post-surgical cancer immunotherapy. *Nat Biomed Eng* 2017;1:0011.
- Zhang X, Wang J, Chen Z, Hu Q, Wang C, Yan J, et al. Engineering PD-1-presenting platelets for cancer immunotherapy. *Nano Lett* 2018;18:5716–25.
- Han X, Chen J, Chu J, Liang C, Ma Q, Fan Q, et al. Platelets as platforms for inhibition of tumor recurrence post-physical therapy by delivery of anti-PD-L1 checkpoint antibody. *J Control Release* 2019;304:233–41.
- Ay C, Simanek R, Vormittag R, Dunkler D, Alguei G, Koder S, et al. High plasma levels of soluble P-selectin are predictive of venous thromboembolism in cancer patients: results from the Vienna cancer and thrombosis study (CATS). *Blood* 2008;112:2703–8.
- Hu Q, Sun W, Qian C, Wang C, Bomba HN, Gu Z. Anticancer platelet-mimicking nanovehicles. *Adv Mater* 2015;27:7043–50.
- Mai X, Zhang Y, Fan H, Song W, Chang Y, Chen B, et al. Integration of immunogenic activation and immunosuppressive reversion using mitochondrial-respiration-inhibited platelet-mimicking nanoparticles. *Biomaterials* 2020;232:119699.
- Hu Q, Qian C, Sun W, Wang J, Chen Z, Bomba HN, et al. Engineered nanoplatelets for enhanced treatment of multiple myeloma and thrombus. *Adv Mater* 2016;28:9573–80.
- Mackman N. Triggers, targets and treatments for thrombosis. *Nature* 2008;451:914–8.
- Modery CL, Ravikumar M, Wong TL, Dzuricky MJ, Durongkaveroj N, Gupta AS. Heteromultivalent liposomal nanoconstructs for enhanced targeting and shear-stable binding to active platelets for site-selective vascular drug delivery. *Biomaterials* 2011;32:9504–14.
- Huang Y, Yu L, Ren J, Gu B, Longstaff C, Hughes AD, et al. An activated-platelet-sensitive nanocarrier enables targeted delivery of tissue plasminogen activator for effective thrombolytic therapy. *J Control Release* 2019;300:1–12.
- Zhang Y, Zhu X, Chen X, Chen Q, Zhou W, Guo Q, et al. Activated platelets-targeting micelles with controlled drug release for effective treatment of primary and metastatic triple negative breast cancer. *Adv Funct Mater* 2019;29:1806620.
- Song J. EMT or apoptosis: a decision for TGF-β. *Cell Res* 2007;17:289–90.
- Massagué J, Obenauf AC. Metastatic colonization by circulating tumour cells. *Nature* 2016;529:298–306.
- Yingling JM, Blanchard KL, Sawyer JS. Development of TGF-β signalling inhibitors for cancer therapy. *Nat Rev Drug Discov* 2004;3:1011–22.
- Metelli A, Wu BX, Riesenber B, Guglietta S, Huck JD, Mills C, et al. Thrombin contributes to cancer immune evasion via proteolysis of platelet-bound GARP to activate LTGF-β. *Sci Transl Med* 2020;12:eaay4860.
- Rouzet F, Bachelet-Violette L, Alsac JM, Suzuki M, Meulemans A, Louedec L, et al. Radiolabeled fucoidan as a P-selectin targeting agent for *in vivo* imaging of platelet-rich thrombus and endothelial activation. *J Nucl Med* 2011;52:1433–40.
- Juenet M, Aid-Launais R, Li B, Berger A, Aerts J, Ollivier V, et al. Thrombolytic therapy based on fucoidan-functionalized polymer nanoparticles targeting P-selectin. *Biomaterials* 2018;156:204–16.
- Li B, Aid-Launais R, Labour MN, Zenych A, Juenet M, Choqueux C, et al. Functionalized polymer microbubbles as new molecular ultrasound contrast agent to target P-selectin in thrombus. *Biomaterials* 2019;194:139–50.
- Li B, Juenet M, Aid-Launais R, Maire M, Ollivier V, Letourneur D, et al. Development of polymer microcapsules functionalized with fucoidan to target P-selectin overexpressed in cardiovascular diseases. *Adv Healthc Mater* 2017;6:1601200.
- Li J, Chen K, Li S, Feng J, Liu T, Wang F, et al. Protective effect of fucoidan from *Fucus vesiculosus* on liver fibrosis via the TGF-β1/Smad pathway-mediated inhibition of extracellular matrix and autophagy. *Drug Des Dev Ther* 2016;10:619–30.
- Fitton JH, Stringer DN, Karpinic SS. Therapies from fucoidan: an update. *Mar Drugs* 2015;13:5920–46.
- Jin JO, Zhang W, Du JY, Wong KW, Oda T, Yu Q. Fucoidan can function as an adjuvant *in vivo* to enhance dendritic cell maturation and function and promote antigen-specific T cell immune responses. *PLoS One* 2014;9:e99396.
- Chiang CS, Lin YJ, Lee R, Lai YH, Cheng HW, Hsieh CH, et al. Combination of fucoidan-based magnetic nanoparticles and immunomodulators enhances tumour-localized immunotherapy. *Nat Nanotechnol* 2018;13:746–54.
- Chen S, Li D, Du X, He X, Huang M, et al. Carrier-free nanoassembly of doxorubicin prodrug and siRNA for combinationally inducing immunogenic cell death and reversing immunosuppression. *Nano Today* 2020;35:100924.
- Lin RJ, Afshar-Kharghan V, Schafer AI. Paraneoplastic thrombocytosis: the secrets of tumor self-promotion. *Blood* 2014;124:184–7.

40. Mitsui C, Kajiwara K, Hayashi H, Ito J, Mita H, Ono E, et al. Platelet activation markers overexpressed specifically in patients with aspirin-exacerbated respiratory disease. *J Allergy Clin Immunol* 2016;137:400–11.
41. Shamay Y, Elkabets M, Li H, Shah J, Brook S, Wang F, et al. P-selectin is a nanotherapeutic delivery target in the tumor microenvironment. *Sci Transl Med* 2016;8:345ra87.
42. Tang H, Chen H, Jia Y, Liu X, Han Z, Wang A, et al. Effect of inhibitors of endocytosis and NF- κ B signal pathway on folate-conjugated nanoparticle endocytosis by rat Kupffer cells. *Int J Nanomed* 2017;12:6937–47.
43. Tang Y, Wang X, Li J, Nie Y, Liao G, Yu Y, et al. Overcoming the reticuloendothelial system barrier to drug delivery with a “don’t-eat-us” strategy. *ACS Nano* 2019;13:13015–26.
44. Dupre SA, Hunter KW. Murine mammary carcinoma 4T1 induces a leukemic reaction with splenomegaly: association with tumor-derived growth factors. *Exp Mol Pathol* 2007;82:12–24.
45. Sceneay J, Chow MT, Chen A, Halse HM, Wong CSF, Andrews DM, et al. Primary tumor hypoxia recruits CD11b $^{+}$ /Ly6Cmed/Ly6G $^{+}$ immune suppressor cells and compromises NK cell cytotoxicity in the premetastatic niche. *Cancer Res* 2012;72:3906–11.
46. Tabariès S, Ouellet V, Hsu BE, Annis MG, Rose AAN, Meunier L, et al. Granulocytic immune infiltrates are essential for the efficient formation of breast cancer liver metastases. *Breast Cancer Res* 2015;17:45.
47. Long Y, Lu Z, Xu S, Li M, Wang X, Zhang Z, et al. Self-delivery micellar nanoparticles prevent premetastatic niche formation by interfering with the early recruitment and vascular destruction of granulocytic myeloid-derived suppressor cells. *Nano Lett* 2019;20:2219–29.
48. Lindau D, Gielen P, Kroesen M, Wesseling P, Adema GJ. The immunosuppressive tumour network: myeloid-derived suppressor cells, regulatory T cells and natural killer T cells. *Immunology* 2013;138:105–15.